Article

1,2-H versus 1,2-C-shift on Sn-Silsesquioxanes

Tyler Ray Josephson, Stephen K Brand, Stavros Caratzoulas, and Dionisios G. Vlachos

ACS Catal., **Just Accepted Manuscript** • DOI: 10.1021/acscatal.6b03128 • Publication Date (Web): 15 Nov 2016

1,2-H versus 1,2-C-shift on Sn-Silsesquioxanes

Tyler R. Josephson[1], Stephen K. Brand[2], Stavros Caratzoulas[3*], Dionisios G. Vlachos[1,3]

[1]*Department of Chemical and Biomolecular Engineering, University of Delaware, Newark, DE 19716*

[2]*Division of Chemistry and Chemical Engineering, California Institute of Technology, Pasadena, CA 91125*

[3]*Catalysis Center for Energy Innovation, University of Delaware, Newark, DE 19716*

[*]*Corresponding author: cstavros@udel.edu*

ABSTRACT

Lewis-acidic zeolites such as Sn-Beta catalyze glucose isomerization to fructose via an intramolecular 1,2-H-shift reaction, a key step for converting lignocellulosic biomass into renewable chemicals. Na-exchange of Sn-Beta titrates the neighboring SiOH group in the open Sn site, and shifts catalyst selectivity to mannose formed by a 1,2-C-shift reaction. To probe structure/activity relationships in the zeolite, tin-containing silsesquioxanes with (**1a**) and without (**1b**) a neighboring SiOH group were recently synthesized and tested. These molecular catalysts are active for glucose conversion, and the presence (absence) of the SiOH favors fructose (mannose) selectivity by intramolecular H(C)-shift reactions. Using density functional theory, we investigated numerous H/C-shift pathways on these tin-silsesquioxane catalysts. On both **1a** and **1b,** the H-shift reaction occurs through a bidentate binding mode without participation of the SiOH, while the bidentate binding mode is not favored for the C-shift due to steric hindrance. Instead, the C-shift reaction occurs through different concerted reaction pathways, in which an acetylacetonate (acac) ligand interacts with the substrate in the transition state complexes. Favorable H-shift pathways without SiOH participation and acac ligand promotion of the C-shift pathway explain why **1a** produces mannose from C-shift reactions instead of exclusively catalyzing H-shift reactions, as the Sn-Beta open site does.

Keywords: silsesquioxanes, zeolites, Lewis acids, hydride transfer, Bilik reaction, Bader

1. INTRODUCTION

Utilization of lignocellulosic biomass as a renewable chemical feedstock is a promising path to a more sustainable chemical industry.[1–5] Lewis-acidic zeolites, Sn-Beta in particular, have emerged as useful catalysts for a wide range of transformations in biomass conversion, including Baeyer-Villiger oxidation of ketones to lactones[6], the Meerwein-Ponndorf-Verley (MPV) reduction of carbonyls[7], the 1,2-H-shift of glucose[8] and xylose[9], retro-aldol and esterification of sugars to lactates[10], the 1,2-carbon shift of glucose[11] and arabinose[12], and dehydration reactions in the production of renewable aromatics from furans[13].

The isomerization of glucose to fructose is of particular interest due to the abundance of cellulose as a glucose feedstock and the value of fructose for production of 5-hydroxymethylfurfural (HMF)[14] and lactic acid[15,16]. ^{119}Sn NMR[11] and acetonitrile adsorption and spectroscopy[17] have identified two types of Sn sites in Sn-Beta: a "closed" framework Sn site, $Sn(OSi)_4$, and a hydrolyzed "open" site, $Sn(OSi)_3OH$ with a neighboring SiOH. Open sites are stronger Lewis acids than closed sites[17–19] and more active for glucose isomerization[18,19]. Figure 1 shows a reaction scheme for different glucose transformation reactions catalyzed by Sn-Beta. Sn-Beta selectively produces fructose F1 via a 1,2-H-shift reaction from glucose, and mannose M1 as a side product via a subsequent 1,2-H-shift reaction from fructose.[18] Modification of the open site by Na^+ titration[18] or with borate salts[12] shifts selectivity from fructose to mannose, but this mannose is produced via a 1,2-C-shift (M2), or Bilik reaction[20]. Moreover, different synthesis methods produce catalysts with different ratios of open and closed sites[17,19]. Understanding these structure-activity and structure-selectivity relationships is important for optimizing Sn-Beta synthesis and deployment in future biorefineries.

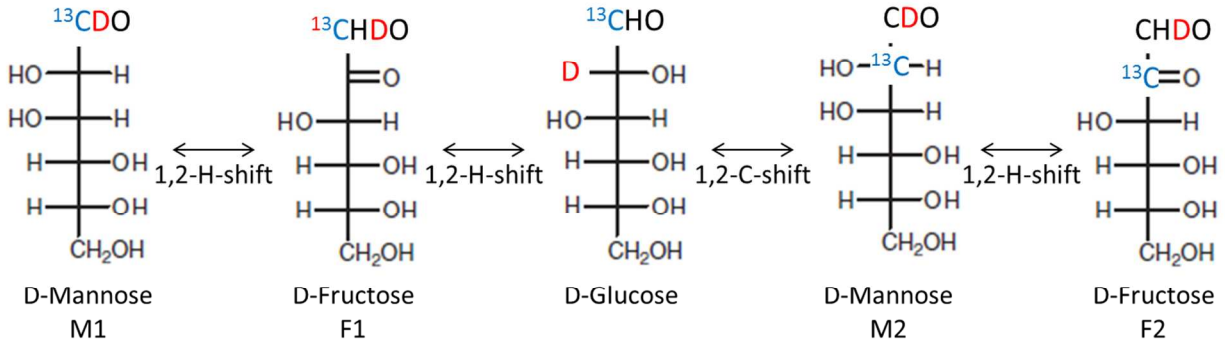

Figure 1. Glucose transformation products via 1,2-H-shift and 1,2-C-shift reactions. Experiments with ^{13}C- and D-labelled glucose enable distinction of mannose and fructose from different pathways.

Beginning with Assary and Curtiss' examination of glyceraldehyde isomerization to dihydroxyacetone on open and closed sites of Sn-Beta,[21] several computational studies have investigated the glucose isomerization mechanism on the Sn-Beta zeolite.[22–27] These have found that the open site is more active than the closed site, whether examined as a 5T (five tetrahedral atoms) cluster[21,22], or an extended 208T QM/MM model[26], implicating the stronger Brønsted basicity of SnOH relative to SnOSi[26]. However, a study using periodic DFT found little difference between closed and open sites[24]. Using a 9T open site cluster, Rai et al. found that glucose in a bidentate coordination to the Sn favored a C-shift reaction, while glucose coordinated to the Sn and neighboring SiOH favored the H-shift reaction, suggesting the neighboring SiOH enabling fructose selectivity by participating in a concerted reaction[25]. However, a more complete analysis of this 9T cluster[27] with and without Na-exchange identified a more favorable bidentate binding geometry that favored the H-shift without SiOH participation, instead finding that Na^+ provides electrostatic stabilization of the C-shift TS more than the H-shift TS. A larger, less flexible zeolite cluster favored a concerted, rather than bidentate, mechanism for both Sn-Beta and Na-Sn-Beta, and observed the same electrostatic effect on the H/C-shift transition states.

These studies highlight several challenges associated with modeling Sn-Beta. In addition, there is no experimental consensus for the crystallographic location of the Sn atom. Consequently, computational studies have used either the T2 substitution[24,26], as it is most thermodynamically stable closed site[28], or the T9 substitution[25,27,29], in agreement with acetonitrile adsorption and spectroscopic evidence[17,30]. The T5/T6 sites exhibited similar agreement with acetonitrile adsoprtion[17], and have also been proposed on account of EXAFS experiments[31], but haven't been examined computationally.

Silsesquioxanes have been useful for reducing the heterogeneous-homogeneous gap in catalysis by providing single-site molecular analogues for evaluating structure-property relationships[32]. Recently, several Sn silsesquioxanes have been synthesized and tested to evaluate the active sites in Sn-Beta[33–36]. Beletskiy et al., synthesized a tetrahedral Sn-silsesquioxane[34], grafted it onto silica[33], and demonstrated its activity for epoxide ring-opening and MPV reduction, comparable to Sn-Beta. This catalyst was also active for glucose isomerization to fructose, but formed significant side products, possibly due to surface silanol groups. Brand et al. have synthesized and tested three tin silsesquioxanes[35,36] (Figure 2)with structural differences designed to model the open (**1a**), Na-exchanged (**1b**), and closed (**2**) sites in Sn-Beta. All catalysts are active for glucose isomerization and epimerization. Analysis of initial rate data for these three tin silsesquioxanes and Sn-Beta, Na-Sn-Beta, and NH_3-Sn-Beta reveals several structure-property correlations among the catalysts.[36] Sn-Beta and **1a** are most active, and selective towards fructose (although mannose formed from Sn-Beta is from a 2,1-H-shift from fructose, while **1a** forms mannose through the 1,2-C-shift of glucose). Na-Sn-Beta and **1b**, each of which have had the neighboring SiOH replaced, showed reduced activity in glucose conversion and a shift in product selectivity to mannose formed by 1,2-C-shift of glucose, implicating the SiOH as an important feature for promoting selectivity to fructose. NH_3-Sn-Beta, CH_3-Sn-Beta, and **2** exhibited an order of magnitude reduction in activity relative to Sn-Beta, with mannose as major product, providing evidence for some residual activity on closed Sn sites. Taken together, these silsesquioxane experiments have decoupled

the functions of the open, closed, and Na-exchanged sites, which cannot be done explicitly in the heterogeneous case due to challenges in synthesizing zeolites with exclusively one kind of Sn site.

In our previous paper, we calculated several pathways for glucose ring-opening, conversion to fructose and mannose, and product ring-closing on **2**[36]. In this work, we report glucose transformation mechanisms for **1a** and **1b**, focusing on the rate-determining steps of the 1,2-H-shift and 1,2-C-shift.

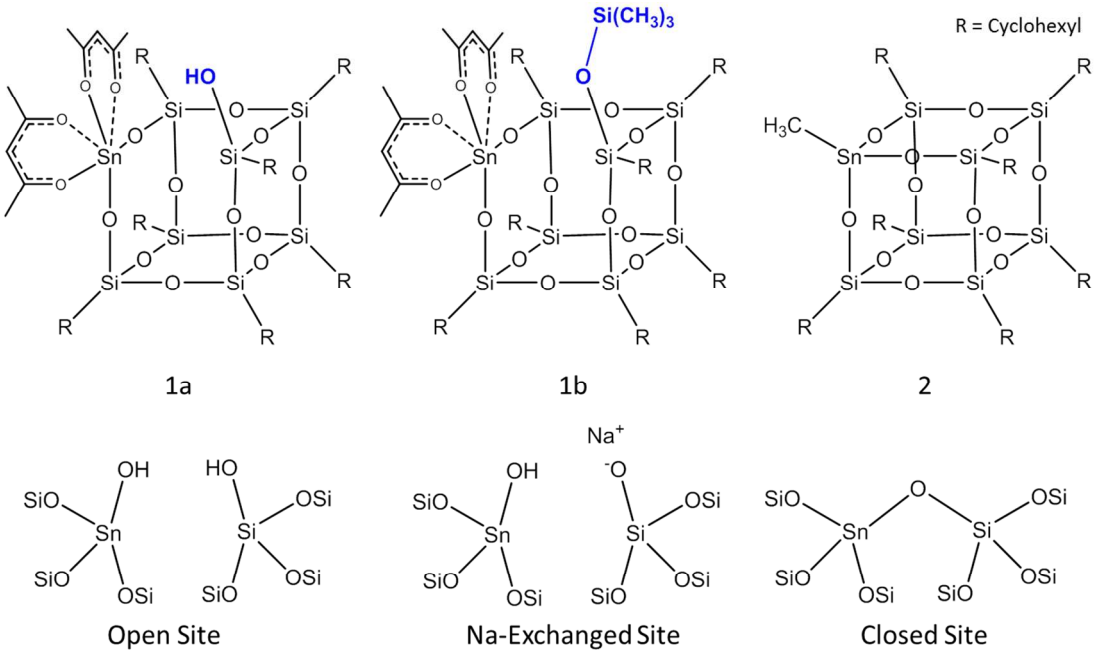

Figure 2. Tin-silsesquioxanes synthesized and tested for glucose isomerization by Brand et al.[35,36] **1a** and **1b** contain an octahedral Sn site, coordinated by two acetylacetonate ligands, and **2** contains a tetrahedral Sn site ligated by a methyl group. These are structural models of the Sn-Beta open, Na-exchanged, and closed sites.

2. COMPUTATIONAL METHODS

Electronic structure calculations were performed using density functional theory to calculate reaction pathways and examine catalyst/substrate interactions. Geometry optimizations and frequency calculations were performed using the M062X functional[37] with the LANL2DZ effective core basis set[38] for the Si and Sn atoms, 3-21G for the cyclohexyl ligands, and 6-31G(d,p) basis set for the sugar, acac ligands, framework O atoms, and the H or CH_3 groups on the SiOH (**1a**) or SiOTMS (**1b**) moieties (basis set A). After geometry optimization, single-point electronic energy calculations with larger basis sets

were performed to refine the calculated electronic energies, using LANL2DZ for Si and Sn, 6-31G(d,p) for the cyclohexyl ligands, and 6-31G(2df,pd) for the sugars, acac ligands, framework O atoms, and H/TMS (basis set B). Transition states were verified by identifying a single imaginary frequency, and reactants and products were connected to transition states by following the intrinsic reaction coordinate. Calculations were performed in the gas phase using Gaussian 09 version A.09[39]; Natural Bond Orbital (NBO) analysis was performed with NBO version 6.0[40]; and analysis using Bader's Atoms-In-Molecules theory (QTAIM)[41] was performed using Critic2[42].

3. RESULTS

3.1 Catalyst Structure. To investigate the stability of the Sn-O interactions with the acac ligands, we examined several possible conformations of **1a** and **1b** (Figure 3). Both **1a** and **1b** were most stable with both acac ligands in the *cis* orientation; significant energy penalties (>20 kcal/mol) are incurred by pulling one or both ligands into the *trans* orientation. Several alternative conformations for **1a** were considered by deprotonating the SiOH to a ligand and forming a third Sn-O-Si bridge. When the proton was transferred to C3 of the acac (forming a diketone) or to an acac O (forming an enol), the resulting structures were significantly less stable than the original structure, because the SiOH is not strongly acidic and the acac ligand is not a strong proton acceptor (see below). An additional configuration was 3.7 kcal/mol less stable than the original structure. In this, the SiOH coordinates to the Sn and H-bonds to the displaced *cis* acac ligand. The dominant Lewis structure of the Sn site in the most stable configuration, according to NBO analysis, is presented in Figure S1.

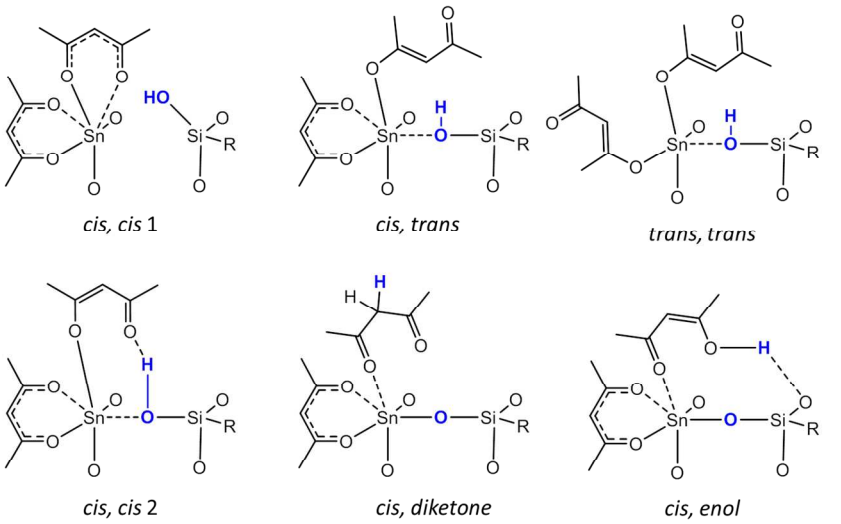

Conformation	1a	1b
cis, cis 1	0.0	0.0
cis, trans	25.2	24.7
trans, trans	54.9	49.9
cis, cis 2	8.44	N/A
cis, diketone	24.9	N/A
cis, enol	8.78	N/A

Figure 3. Different orientations of acac ligands on Sn in **1a** and **1b**, with relative free energies at 353 K reported in kcal/mol.

3.2 Proton Affinities. Both the 1,2 H-shift and 1,2 C-shift reactions are activated by an initial deprotonation of the substrate.[23] In addition, the Brønsted basicity of the SnOH in Lewis-acidic zeolites has been proposed as a descriptor for the 1,2 H-shift barrier.[26] To probe the relative strength of candidate Brønsted bases, proton affinities were calculated for several sites on the catalyst (Figure 4). The Sn-O-Si bridge oxygens bound the proton most strongly, with proton affinities of 242 kcal/mol for both **1a** and **1b**. In **1a**, a proton placed on the SiOH migrated to the Sn-O-Si bridge during optimization, while in **1b**, a proton placed on the SiOTMS was shared with a ligand oxygen. The proton affinities of the ligand oxygens (O4-O7) were considerably less favorable – ranging from 217.0 to 222.3 kcal/mol – and in several cases, the proton migrated away from the ligand O to another O during optimization. The third carbon of each acac ligand also had weaker proton affinities (ranging from 217.7 to 229.7 kcal/mol). We therefore rule out the acac ligands as proton acceptors in sugar deprotonation.

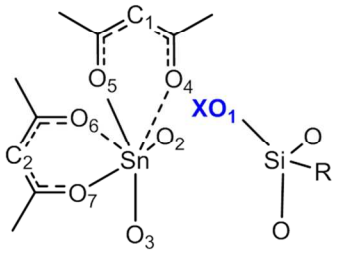

Protonation Site	1a Proton Affinity (kcal/mol)	1b Proton Affinity (kcal/mol)
$O_{1\,c}$	239.8 [a]	237.2 [c]
O_2	240.2	241.9
O_3	235.3	239.5
O_4	242.0 [a]	220.3
O_5	219.9	217.6
O_6	217.0	222.3
$O_{/\,b}$	239.0 [b]	238.4 [b]
C_1	217.7	220.5
C_2	224.7	229.7

Figure 4. Proton affinities of candidate Brønsted bases in **1a** (X=H) and **1b** (X=Si$(CH_3)_3$). [a] Proton migrated to bridge O2 during optimization; shared with SiOH. [b] Proton migrated to Si-O-Si bridge; shared with ligand O7 [c] Proton on OTMS; shared with ligand O7

3.3 Reaction Pathways. To reduce configurational complexity, accelerate calculations, and focus on the salient features of the reaction mechanism, we approximated glucose as glyceraldehyde (GLY), the smallest aldose which allows for comparison of the 1,2-H-shift and 1,2-C-shift reactions, producing dihydroxyacetone (DHA) and GLY with opposite chirality to the reactant, respectively.

The 1,2 hydride/carbon shift reaction on a bifunctional Lewis acid/Brønsted base active site can be generalized to three possible mechanisms, depending on the binding geometry to the site.[36] The "bidentate binding" pathway, so-named for the bidentate coordination of the sugar at the transition state, involves three steps: 1) deprotonation of O2 to the Brønsted base and binding of O2 to the Lewis acid, 2) the H/C-shift reaction in a chelate-like transition state, and 3) reprotonation of O1. The "O1 binding" pathway is two steps: concerted deprotonation with the H/C-shift, followed by reprotonation. The "O2 binding" pathway is also two steps: deprotonation of O2 to the Brønsted base and subsequent H/C-shift concerted with reprotonation. Only 6 pathways are needed to examine a catalyst with a single Lewis-acid/Brønsted base site, the methyl-tin silsesquioxane **2**, with only the Sn-O-Si bridge moiety. While **1b** has only Sn-O-Si bridges as Brønsted bases, allowing for 6 distinct pathways, **1a** has Sn-O-Si

bridges as well as a SiOH, which may facilitate proton transfers to the Sn-O-Si bridges or to the acac ligands, as has been proposed for Sn-Beta.[25,27]

3.3.1 Pathways on Sn-O-Si bridges. Figure 5 depicts the pathways on the Sn-O-Si bridges, and Table S1 and Figures S2-S4 contain the energetics for these pathways on **1a** and **1b**. Figure 8 gives the highest TS free energy for all pathways to facilitate their comparison. For a 1,2-H-shift reaction, the product is DHA, and R_1 and R_2 designate H and CH_2OH, respectively. For a 1,2-C-shift reaction, the product is GLY of opposite chirality, and R_1 and R_2 designate CH_2OH and H, respectively.

The bidentate binding pathway begins by deprotonating GLY to a Sn-O-Si bridge, binding O2 of GLY to the Sn and forming a new silanol by virtue of the opening of the Sn-O-Si bridge. At intermediate B-3, **1a** has two SiOH groups, while **1b** has this new SiOH and the original SiOTMS. The highest transition state in these pathways was B-4, with the H-shift being favored over the C-shift on both **1a** (TS free energies of 28.3 and 32.8 kcal/mol, respectively) and **1b** (27.5 and 38.1 kcal/mol). The higher barrier for the C-shift is due to greater steric hindrance by the acac ligands on the transferring CH_2OH group compared to the H. Christianson et al., also found the bidentate-binding C-shift TS to be less stable than that for the H-shift on Sn-Beta[27].

The bidentate binding pathways contain configurations unique to this work in their unusually crowded 7-coordinated Sn. In Sn-Beta, both closed and open sites are tetrahedral when all water ligands have been removed, 5-coordinated with NH_3 adsorbed, and octahedral when water is adsorbed.[18] In aqueous solution, the coordination of Sn(IV) is 6,[43] as $[Sn(OH_2)_6]^{4+}$, but higher coordination has not been observed. Furthermore, while bidentate binding is possible in relatively flexible zeolite clusters,[22,25,27] it is unfavorable in larger, less flexible clusters and periodic zeolite models[26,27] in which the open site is formed by hydrolyzing a Sn-O-Si. For these reasons, we were not expecting to find a favorable bidentate binding mode in **1a** and **1b**, yet it is not only possible, but most favorable for H-shift pathways. In order

to accommodate the sugar oxygens at the TS, the ligand and framework oxygens are displaced, and the average Sn-O(acac) distance increases slightly from 2.052 Å in isolated **1a** to 2.122 Å at the bidentate H-shift TS on **1a**. An octahedral Sn ideally contains O-Sn-O angles of 90°, and **1a** and **1b** have angles ranging from 84.5° between oxygens on the same ligand, and 101.2° between a framework and ligand O. However, in the bidentate H-shift TS, for example, the coordinated oxygens form a pentagonal bipyramid with O-Sn-O angles ranging from 70.7° to 76.4° in the plane of the pentagon – near the ideal value of 72°. While the bidentate H-shift is the most stable H-shift pathway, the bidentate C-shift is unfavorable due to its bulkier transition state; the steric hindrance imposed by the acac ligands results in more favorable monodentate binding for the C-shift.

The O1-binding pathway begins by coordinating O1 to the Sn and the O2 hydroxyl into an H-bond with a Sn-O-Si bridge. This either requires bringing Sn into a 7-coordinated arrangement (O1 H/C-shift on **1a**, and O1 H-shift on **1b)** or displacing an O of the acac ligand (O1 C-shift on **1b**). O2 is then deprotonated to form a silanol in a concerted reaction with the H/C-shift. The final step is reprotonation of O1 from the newly formed silanol. On **1a**, both the H-shift and C-shift TS were considerably less stable than in the bidentate binding mode (16 and 9 kcal/mol higher energy, respectively), but on **1b**, the O1-binding C-shift TS was more stable than the bidentate binding TS by 10 kcal/mol). This stabilization occurs due to reduced crowding around the Sn site and interactions between the O3 hydroxyl and acac ligand oxygens (see Discussion and Supporting Information).

The O2-binding pathway begins by deprotonating the O2 hydroxyl to a Sn-O-Si bridge and opening of the latter. The formyl O1 forms an H-bond with the newly-formed silanol, and in the next step, the silanol transfers its proton to O1 in a concerted step with the H/C-shift, forming the final product. None of the O2 binding pathways were found to be the most favorable on 1a or 1b.

The Sn-O-Si bridge pathways comprise the possible pathways on **1b**, and we can identify an important effect of the SiOH replacement with SiOTMS. On **1a**, the bidentate H-shift is favored over the C-shift by 4.5 kcal/mol, while on **1b**, the H-shift is even more favored, by 7.6 kcal/mol; in this case, the bulky TMS crowds the ligands, which cannot displace as much to accommodate the bulky C-shift TS. On the other hand, the O1-binding pathway on **1b** significantly stabilizes the C-shift, while it does not on **1a**. This brings the difference between the most favorable pathways on **1b**, the bidentate H-shift and the O1 binding C-shift, to less than 1 kcal/mol, within typical DFT errors.

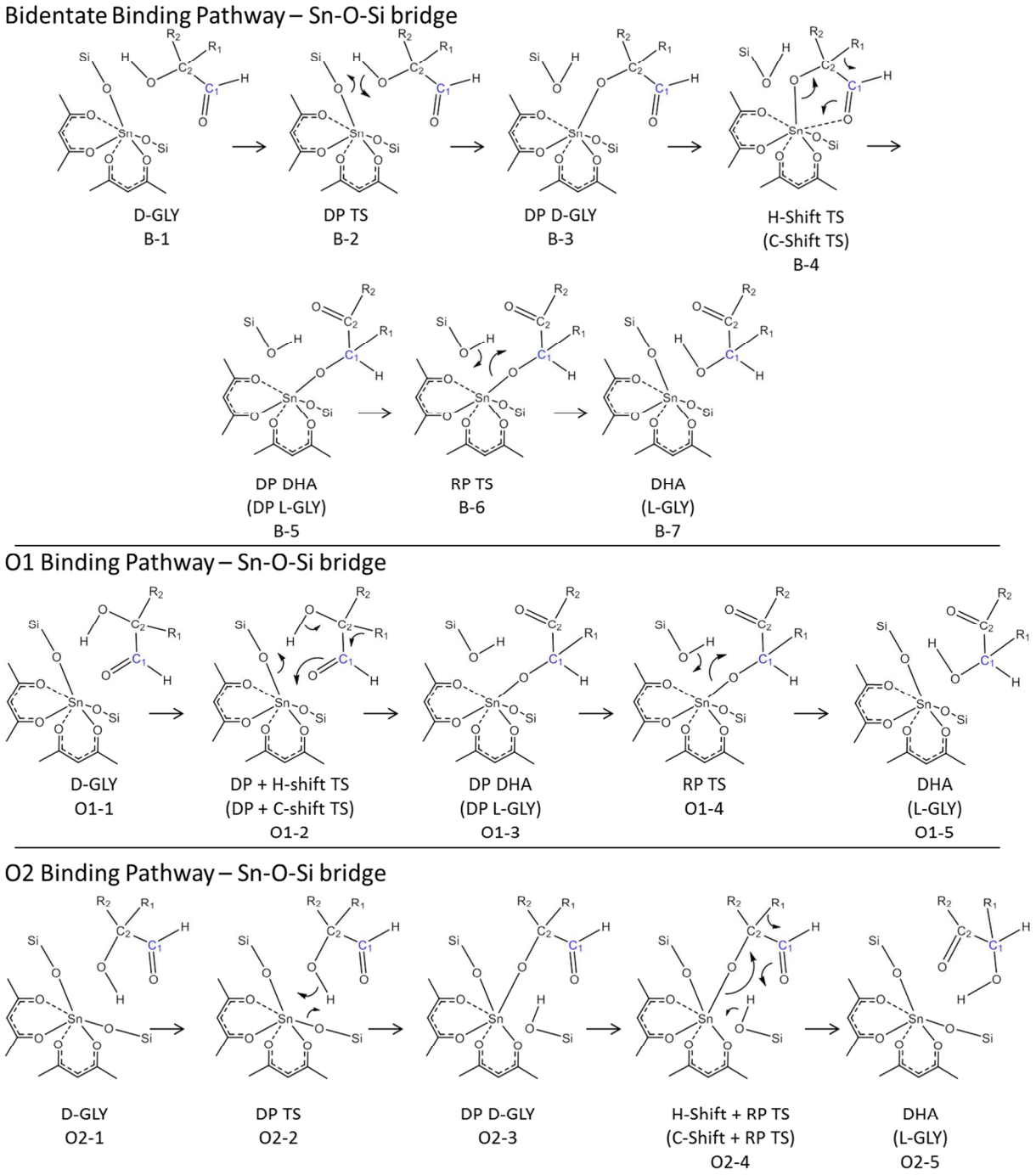

Figure 5. Reaction pathways for H/C-shift on Sn-O-Si bridge in **1a** and **1b**. GLY = glyceraldehyde, DHA = dihydroxyacetone, DP = deprotonation, RP = reprotonation. When R_1 = H, R_2 = CH_2OH, the rate-determining step contains a H-shift, and the product is DHA. When R_1 = CH_2OH, R_2 = H, the rate-determining step contains a C-shift, and the product is glyceraldehyde of opposite chirality to the reactant.

3.3.2. Pathways unique to 1a. The silanol function on **1a** enables additional reaction pathways by facilitating proton transfers during the H/C-shift steps and by permitting the *cis,cis 2* configuration of **1a**, allowing participation of a ligand oxygen. We identified O1 and O2 binding pathways with the SiOH acting as the proton acceptor/donor, facilitating a proton transfer with either a Sn-O-Si bridge or with a ligand O, as well as a pathway in which a displaced acac ligand stabilizes the H/C-shift transition state by interacting with the transferring moiety. These pathways are shown in Figure 6 and Figure 7; energetics are reported in **Error! Reference source not found.** and Figures S5 and S6, and the highest TS energy for each pathway is shown in Figure 8.

In the O1sb and O2sb pathways, GLY approaches the Sn site on the same side as the SiOH, and the SiOH participates by shuttling a proton to a Sn-O-Si bridge. In the O1sb pathways, the SiOH donates an H-bond across a face of the silicate cube to an opposite Sn-O-Si bridge, and when the GLY undergoes a concerted H-shift and deprotonation, the SiOH acts as a proton "wire," receiving the O2 hydroxyl proton and passing its own proton to the Sn-O-Si bridge. In the O2sb pathways, GLY deprotonates to a Sn-O-Si bridge and binds to the Sn as in the O2 pathways, but the subsequent concerted H-shift/reprotonation uses the SiOH to shuttle the proton to O1. TS energies for all of these pathways were unfavorable, being over 10 kcal/mol greater than H/C-shift TS energies for the bidentate binding mode on **1a**.

Two variations on these pathways were also explored. In these pathways, catalyst **1a** first rearranges to the *cis,cis 2* configuration (see Figure 3). When the sugar binds, the displaced acac ligand O interacts with the O3 hydroxyl of GLY, and HC2, which will undergo the H-shift, is either far from (O1sb-la) or near to (O1sb-lb) the acac O. The H-shift proceeds in a concerted reaction with the SiOH shuttling a proton from O2 to the Sn-O-Si bridge, but the ligand interaction reduces the barrier. In O1sb-la, the ligand oxygen is H-bonded to O3 at the TS, bringing the TS free energy to 38.8 kcal/mol, and in O1sb-lb, the ligand oxygen is coordinated to the transferring H atom, reducing the TS free energy to 32.7

kcal/mol. Having a ligand O stabilizing the transferring H does reduce the barrier, but the bidentate pathway, with a TS energy of 28.3 kcal/mol) remains favored by 4.4 kcal/mol.

We also identified pathways involving the SiOH shuttling a proton to an acac ligand oxygen. These also begin with the catalyst in the *cis,cis 2* configuration, except when the sugar binds, the displaced acac ligand oxygen retains its H-bond with the SiOH. In these pathways, the sugar undergoes an O1-binding pathway, a concerted C-shift with deprotonation to the SiOH, which passes its proton to the ligand O, forming an enol. Reversing this proton shuttle back to the O1 oxygen completes the cycle to produce the product sugar. In both the H- and C-shift reactions, the O3 hydroxyl is interacting with the ligand acac (or enol at O2sl-3), which dramatically reduces the C-shift TS free energy to 28.2 kcal/mol. This is the most favorable C-shift pathway on **1a**, which is comparable in energy to the H-shift, although varying significantly in structure.

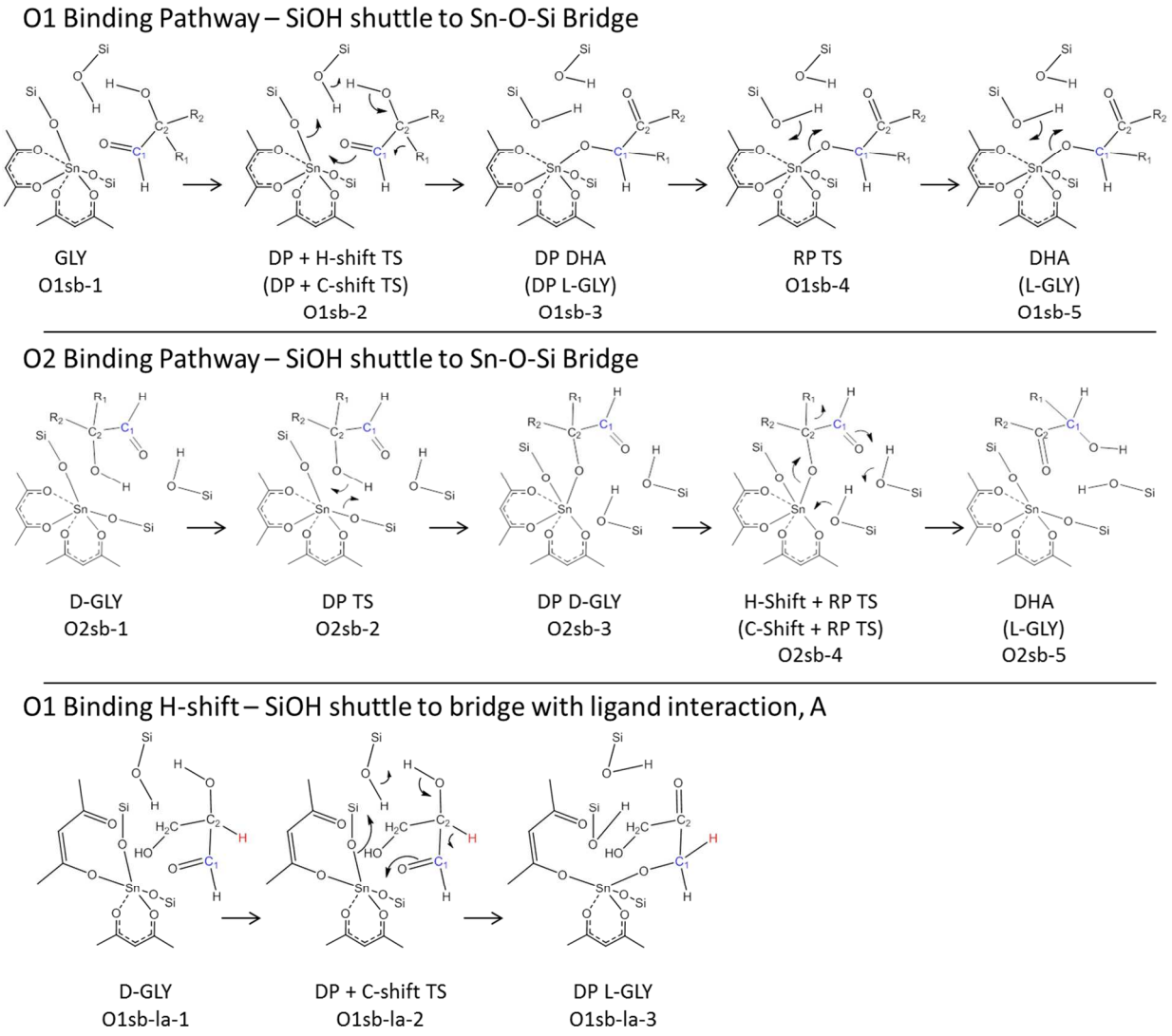

Figure 6. Pathways unique to **1a**, invoking the SiOH in proton transfer to a Sn-O-Si bridge. GLY = glyceraldehyde, DHA = dihydroxyacetone, DP = deprotonation, RP = reprotonation. When R_1 = H, R_2 = CH_2OH, the rate-determining step contains a H-shift, and the product is DHA. When R_1 = CH_2OH, R_2 = H, the rate-determining step contains a C-shift, and the product is glyceraldehyde of opposite chirality to the reactant.

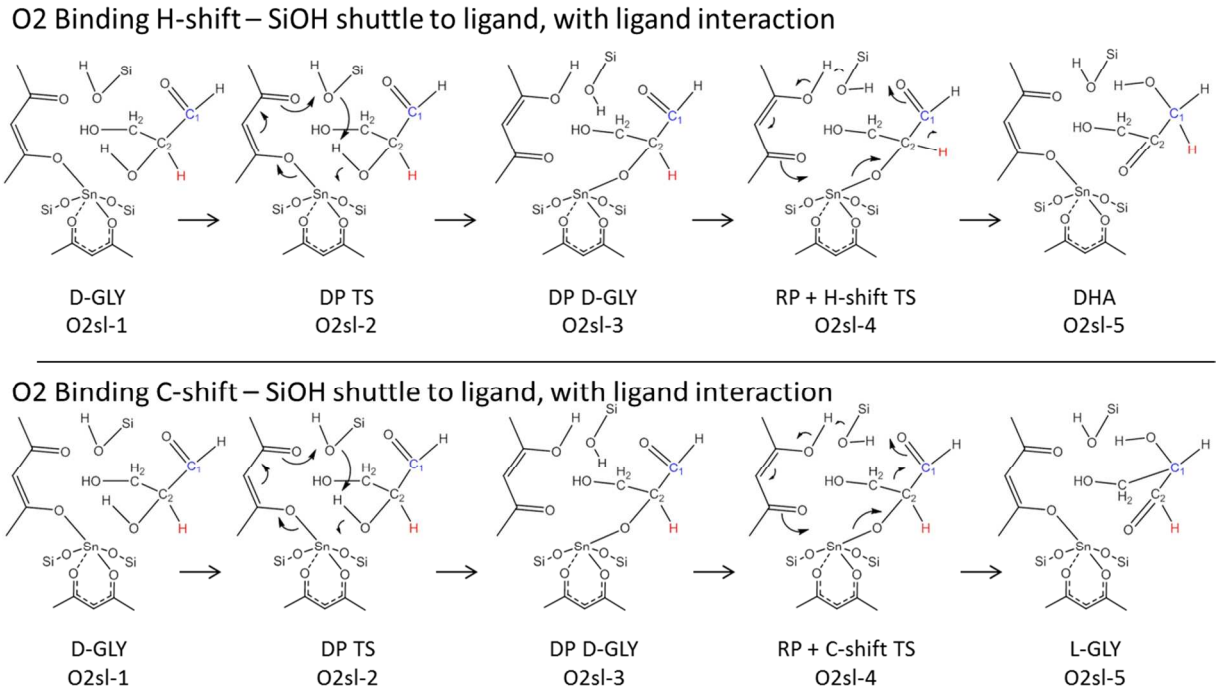

Figure 7. Pathways unique to **1a**, continued, invoking the SiOH in proton transfer to an acac ligand O. GLY = glyceraldehyde, DHA = dihydroxyacetone, DP = deprotonation, RP = reprotonation.

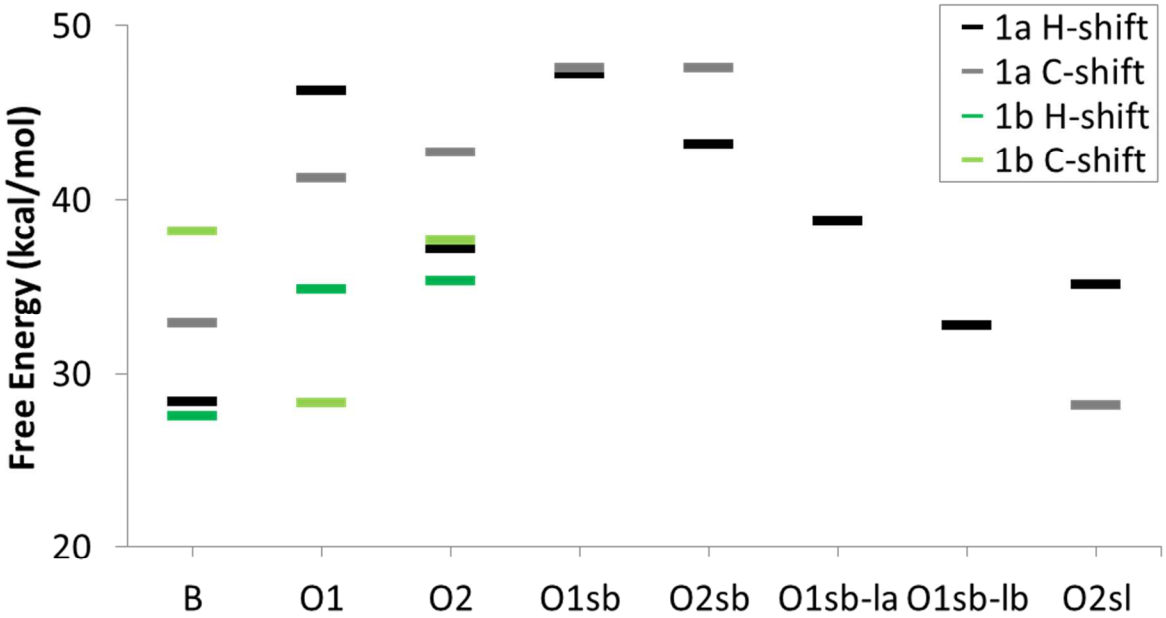

Figure 8 Highest TS free energy of all reaction pathways, calculated at 353 K. Full reaction profiles are reported in Tables S1 and S2 and in Figures S2-S6 in the Supporting Information.

4. DISCUSSION

Overall, the most favorable H-shift TS for both **1a** and **1b** is the bidentate binding mode, with TS free energies of 28.3 and 27.5 kcal/mol, respectively (**Figure 8**).

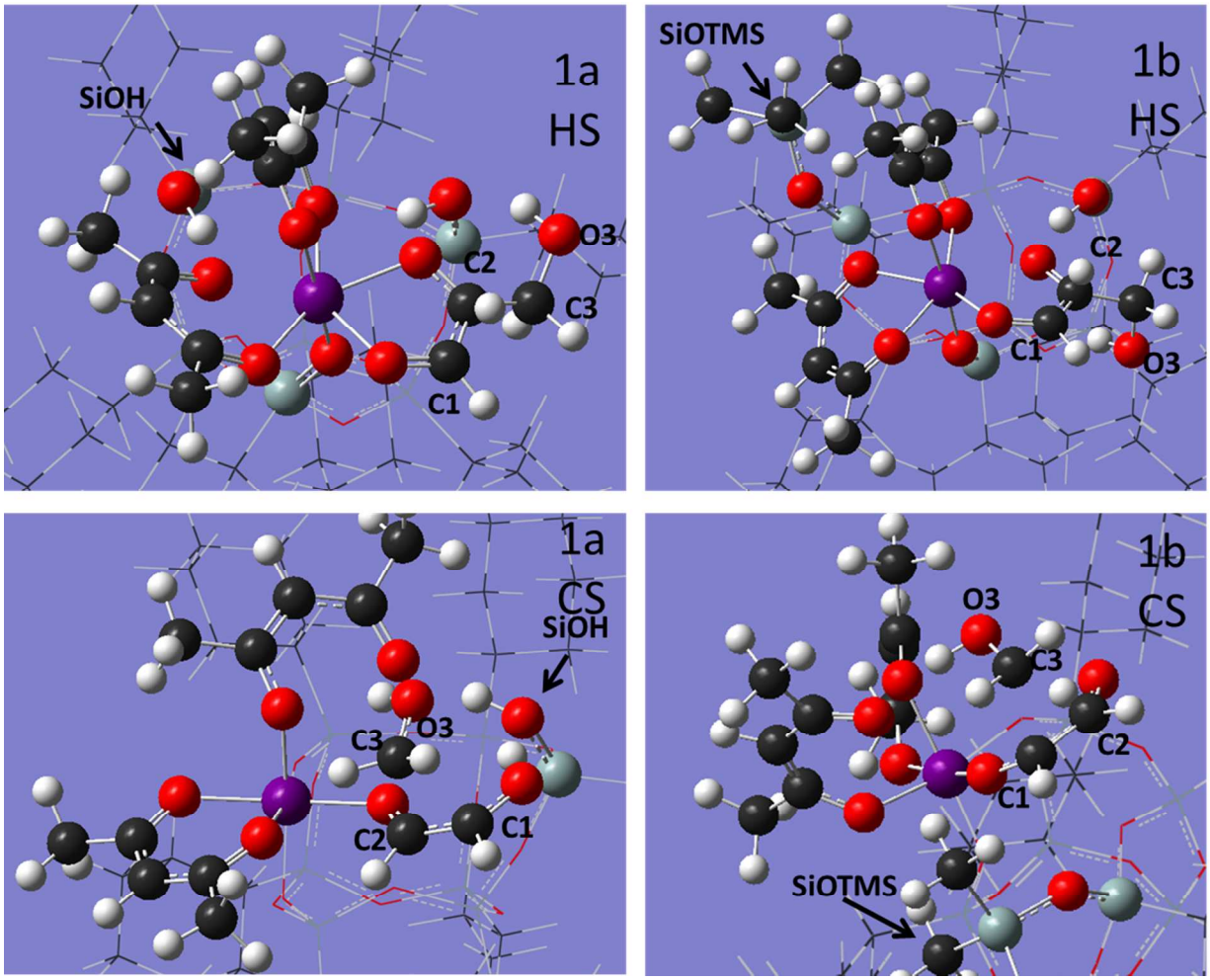

Figure 9 shows images of these geometries. We find that, while the SiOH permits numerous additional pathways on **1a**, none of these are more energetically favorable than the bidentate binding mode, which both **1a** and **1b** can accommodate. Likewise, the most favorable C-shift TS for both **1a** and **1b** have remarkably similar free energies, 28.2 and 28.3 kcal/mol, respectively, even though **1a** involves a concerted proton shuttle from O2 to SiOH to an acac ligand, while **1b** involves a concerted proton transfer to a Sn-O-Si bridge. The common feature in both of these pathways is a strong interaction

between acac ligand oxygen(s) and the O3 hydroxyl at the transition state. Despite the structural diversity among these reaction pathways, the TS energies are indistinguishable, within typical DFT errors.

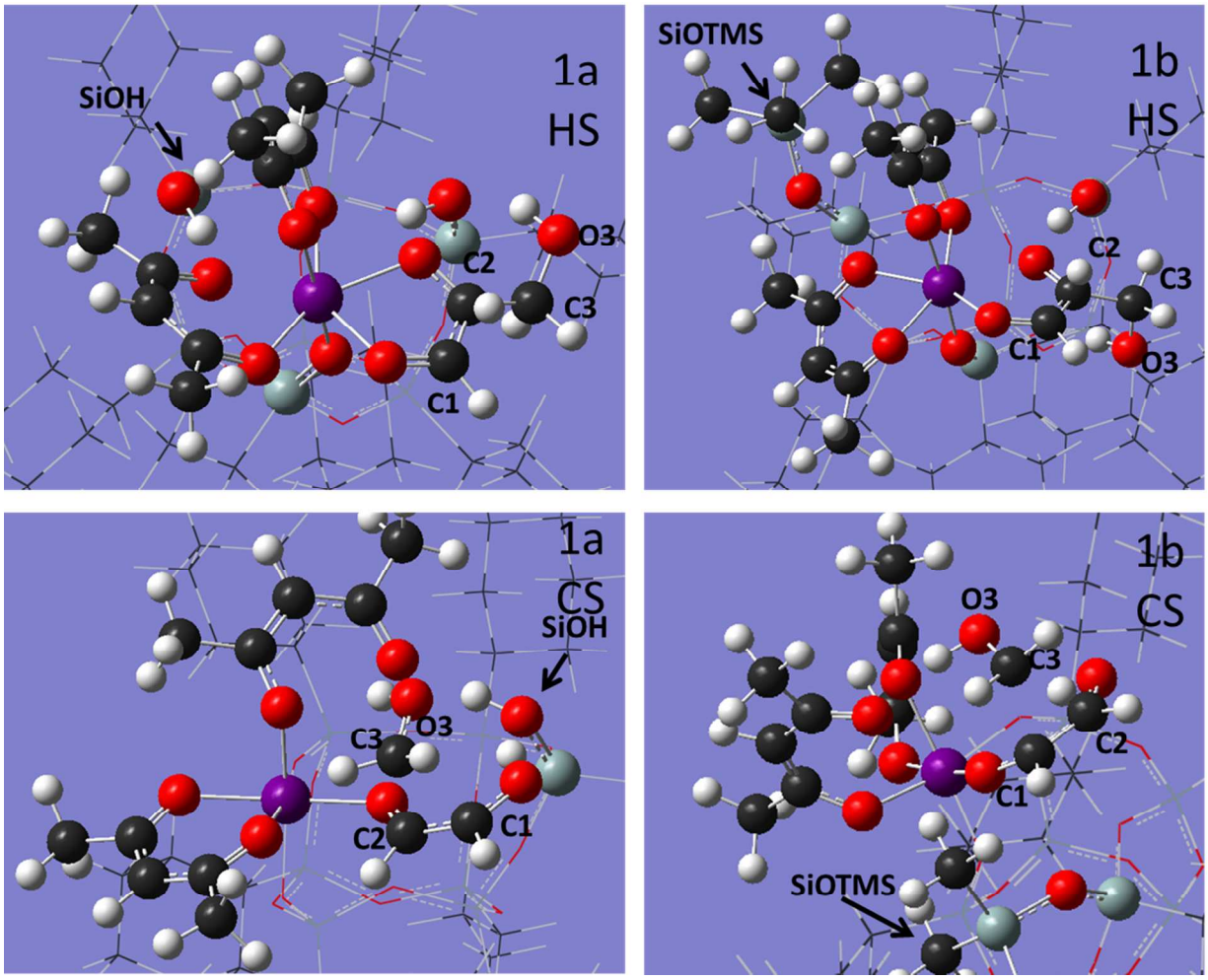

Figure 9. Lowest-barrier transition state geometries for the H/C-shift reaction on 1a and 1b. The sugar, acac ligands, Sn-O-Si bridge atoms, and SiOH/SiOTMS are shown as ball and stick to clarify the active site geometry and to highlight the sugar/catalyst interactions. Coordinates may be found in the Supporting Information as OH_H_B-5, OH_C_O2sl-4, TMS_H_B-5, and TMS_C_O1-2.

One common feature among the most favorable C-shift reactions is an H-bonding interaction between the C3 hydroxyl and an oxygen atom of the catalyst. To examine this more closely, we analyzed several H/C-shift transition states using Bader's Atoms In Molecules (QTAIM) theory[41]. Table S3 in the

Supporting Information provides key information about the (3, -1) bond critical points (BCPs) involved in the H/C-shift elementary steps.

The key interaction identified in the Bader analysis for the C-shift is the contraction of the C3-O3 bond at the TS, which is accompanied by an increase in electron density and charge concentration as the single bond takes on more double-bond character. The lowest-barrier C-shift TS exhibits the most dramatic contraction of the C3-O3 bond, from 1.403 Å in gas phase to 1.333 Å at the O2sl-4 C-shift TS, while the highest-barrier C-shift exhibits less contraction, with a C3-O3 bond length of 1.361 at the C-shift TS. This contraction is accompanied by an increase in charge density ρ, an increase in local charge concentration (marked by a sign change in $\nabla^2(\rho)$), and an increase in bond ellipticity – all signatures of increased double-bond character. This is facilitated by H-bond interactions between the O3 hydroxyl and SiOH, SiOSi, or ligand O in the catalyst, depending on the pathway. In the most favorable C-shift on both 1a and 1b, the O3 hydroxyl is interacting with two ligand oxygens, which stabilize a weakened O3-H bond and a strengthened C3-O3 bond. The activity for both of these catalysts for the C-shift pathway is therefore a consequence of the acac ligands.

According to the Energy Span Model[44] and the Curtin-Hammett Principle[45], the selectivity of a simple reaction network with measured turn-over frequencies (TOF) to two products can be expressed as

$$S = \frac{TOF_A}{TOF_B} \approx e^{\Delta G_{TS}} = \mathrm{e}^{\frac{G_{TS,B} - G_{TS,A}}{RT}}$$

where ΔG_{TS} is the difference in Gibbs free energy of the selectivity-determining TS for products A and B.[44] From the experimental data at 353 K, with **1a**, $G_{TS,MAN} - G_{TS,FRU}$ = 0.22 kcal/mol, while with **1b**, $G_{TS,MAN} - G_{TS,FRU}$ = -0.73 kcal/mol (see Table). Both of these free energy differences are less than typical DFT error of ~2 kcal/mol.

Using the energy span model, we also calculated the TOF at 353 K for the lowest-barrier H/C-shift pathways on 1a and 1b. The calculated TOF on **1a** are 1.98 x 10^{-7} mol sugar/s mol Sn for H-shift and 2.48 x 10^{-7} for C-shift; on **1b**, these are 6.01 x 10^{-7} and 2.07 x 10^{-7} respectively. Resolving the difference between experimental and theoretical rates would require reducing the theoretical barriers by about 7 kcal/mol. Such an energy difference can readily be attributed to hydrogen bonding between the hexose substrate and the surrounding solvent molecules (specifically, DMSO), which were not accounted for in this study with the model triose in the gas phase.

Table 1. Experimental initial rate data on **1a** and **1b** from Brand et al.[35,36] and the Gibbs free energy differences between the TOF-determining transition states for fructose and mannose formation assuming constant pre-exponential terms.

	1a	1b
Fructose TOF (mol/s L mol Sn)	0.756	0.134
Mannose TOF (mol/s L mol Sn)	0.549	0.38
TOF_{Fru}/TOF_{Man}	1.38	0.353
ΔG_{TS}	0.320	-1.04
$G_{TS,MAN} - G_{TS,FRU}$ at 353 K (kcal/mol)	0.224	-0.731

Our calculations are consistent with experiment in identifying H-shift and C-shift pathways of comparable barriers on each catalyst. More importantly, we can rule out the hypothesis that SiOH participation in the rate-determining step is critical for fructose selectivity, because H-shift pathways involving SiOH participation (O1sb, O2sb, O1sb-la, O1sb-lb, and O2sl) consistently gave higher barriers than the bidentate H-shift pathway (4.4 kcal/mol higher for O1sb-lb and > 6.9 kcal/mol higher for the others). We also identify the importance of ligand O atom interactions with the O3 for stabilizing the C-shift TS; pathways without this ligand interaction gave higher barriers (4.7 kcal/mol higher for bidentate on **1a** and >9 kcal/mol higher for the others).

1a and **1b** are therefore limited models of the open sites of Sn-Beta and Na-Sn-Beta, in particular due to the presence of the acac ligands, which stabilize the C-shift transition state whether or not a SiOH is present. Sn-Beta is so selective to H-shift reactions that mannose from C-shift is undetected; mannose

is instead produced via a double H-shift. Consequently, the activation of the C-shift pathway by Na-Sn-Beta is a dramatic change. Because **1a** is already active for the C-shift, the shift in selectivity to mannose with the TMS substitution is more incremental. We have identified why this is the case: the acac ligands can stabilize the C-shift TS so that it has comparable barriers to the H-shift on both **1a** and **1b**. As Quadrelli and Basset conclude in their review of silsesquioxanes as analogues to heterogeneous catalysts,[32] "*The analogy [between heterogeneous and silsesquioxane chemistry] mostly breaks down when silsesquioxane can access a chemistry that heterogeneous catalysts cannot*," which we find to be the case in catalysts **1a** and **1b** due to the presence of the acac ligands.

5. CONCLUSIONS

Several pathways were investigated for H-shift and C-shift pathways on the tin-silsesquioxanes **1a** and **1b**. The H-shift proceeds through a bidentate binding pathway on both **1a** and **1b**, and the C-shift proceeds through concerted pathways that invoke the acac ligand. The most favorable H/C-shift pathways on **1a** and **1b** have comparable barriers, consistent with both fructose (from H-shift) and mannose (from C-shift) produced in significant quantities on both catalysts. Our calculations show that the selectivity of the Sn-silsesquioxanes is not determined by the presence (in Sn-silsesquioxane **1a**) or absence (from Sn-silsesquioxane **1b**) of a silanol group SiOH. We find that there is nothing inherent about the silanol group that would tilt the outcome either in the direction of the 1,2-H-shift channel or in the direction of the 1,2-C-shift. Both channels are activated by an initial proton transfer (from the C2-OH) which can take place quite effectively via a Sn-O-Si bridge or an acac ligand. Both channels—in the gas phase—are almost equally accessible. This conclusion should be independent of the theory level, in the sense that it is independent of the error inherent in DFT, since all pathways were computed at the same level. Further, it is in reasonable agreement with the experiments (carried out in mixed, 50/50 v/v benzene/DMSO solvent), according to which isomerization is preferred to epimerization with a TOF ratio of 1.4 on **1a**, while epimerization is preferred to isomerization with a TOF ratio of 2.5 on **1b**. Our

calculations suggest that the modest differences in selectivity between the Sn-silsesquioxanes **1a** and **1b** must be due to micro-solvation phenomena: the trimethylsilyl-capped **1b** is locally less polar in the vicinity of the active site compared to the SiOH-bearing **1a**.

.

ACKNOWLEDGEMENTS

Research was supported as part of the Catalysis Center for Energy Innovation, an Energy Frontier Research Center funded by the U.S. Department of Energy (DOE), Office of Science, Basic Energy Sciences (BES), under Award number DE-SC0001004. This research used resources of the National Energy Research Scientific Computing Center, a DOE Office of Science User Facility supported by the Office of Science of the U.S. Department of Energy under Contract No. DE-AC02-05CH11231. T.R.J. wishes to acknowledge funding from the National Science Foundation Graduate Research Fellowship Program under Grant No. 0750966, as well as the George W. Laird Merit Fellowship. S.K.B. wishes to acknowledge funding from the National Science Foundation Graduate Research Fellowship Program under Grant No. DGE-1144469. Any opinions, findings, and conclusions or recommendations expressed in this material are those of the author(s) and do not necessarily reflect the views of the National Science Foundation. The authors would like to thank Professor Mark Davis and Dr. Jeff Christianson for numerous useful conversations.

Supporting Information Available: Figure S1 gives the Lewis structures of catalysts **1a** and **1b** from NBO analysis. Figures S2 – S6 give free energy profiles for the reaction pathways on **1a** and **1b**. Tables S1 and S2 provide tabulated free energies for all of these optimized intermediates and transition states on **1a** and **1b**. A section describing analysis of key reaction steps using Bader's atoms-in-molecules theory is provided, with analysis of bond critical points provided in Table S3. Also included in the Supporting Information are compressed folders containing .xyz files with the geometries of all optimized

intermediates and transition states. This material is available free of charge via the Internet at http://pubs.acs.org."

REFERENCES

(1) Werpy, T.; Petersen, G. *U.S. Department of Energy* **2004**, *1*, 76.

(2) Ragauskas, A. J.; Williams, C. K.; Davison, B. H.; Britovsek, G.; Cairney, J.; Eckert, C. A.; Frederick, W. J.; Hallett, J. P.; Leak, D. J.; Liotta, C. L.; Mielenz, J. R.; Murphy, R.; Templer, R.; Tschaplinski, T.; Frederick Jr., W. J.; Hallett, J. P.; Leak, D. J.; Liotta, C. L.; Mielenz, J. R.; Murphy, R.; Templer, R.; Tschaplinski, T. *Science* **2006**, *311*, 484–489.

(3) Tilman, D.; Socolow, R.; Foley, J. J. A.; Hill, J.; Larson, E.; Lynd, L.; Pacala, S.; Reilly, J.; Searchinger, T.; Somerville, C.; Williams, R. *Science* **2009**, *325*, 270–271.

(4) Perlack, R. D.; Stokes, B. J. *U.S. Department of Energy,* ORNL/TM-2011/224, Oak Ridge National Laboratory, Oak Ridge, TN **2011**.

(5) Bruijnincx, P. C. A.; Weckhuysen, B. M. *Angew. Chemie - Int. Ed.* **2013**, *52*, 11980–11987.

(6) Corma, A.; Nemeth, L. T.; Renz, M.; Valencia, S. *Nature* **2001**, *412*, 423–425.

(7) Corma, A.; Domine, M. E.; Nemeth, L.; Valencia, S. *J. Am. Chem. Soc.* **2002**, *124*, 3194–3195.

(8) Moliner, M.; Roman-Leshkov, Y.; Davis, M. E. E.; Román-Leshkov, Y.; Davis, M. E. E. *Proc. Natl. Acad. Sci. U.S.A.* **2010**, *107*, 6164–6168.

(9) Choudhary, V.; Pinar, A. B.; Sandler, S. I.; Vlachos, D. G.; Lobo, R. F. *ACS Catal.* **2011**, *1*, 1724–1728.

(10) Holm, M. S.; Saravanamurugan, S.; Taarning, E. *Science* **2010**, *328*, 602–605.

(11) Bermejo-Deval, R.; Gounder, R.; Davis, M. E. *ACS Catal.* **2012**, *2*, 2705–2713.

(12) Gunther, W. R.; Wang, Y.; Ji, Y.; Michaelis, V. K.; Hunt, S. T.; Griffin, R. G.; Román-Leshkov, Y. *Nat.*

Commun. **2012**, *3*, 1109.

(13) Williams, C. L.; Chang, C.-C.; Do, P.; Nikbin, N.; Caratzoulas, S.; Vlachos, D. G.; Lobo, R. F.; Fan, W.; Dauenhauer, P. J. *ACS Catal.* **2012**, *2*, 935–939.

(14) Van Putten, R. J.; Van Der Waal, J. C.; De Jong, E.; Rasrendra, C. B.; Heeres, H. J.; De Vries, J. G. *Chem. Rev.* **2013**, *113*, 1499–1597.

(15) Orazov, M.; Davis, M. E. *Proc. Natl. Acad. Sci.* **2015**, *112*, 201516466.

(16) Dusselier, M.; Van Wouwe, P.; Dewaele, A.; Makshina, E.; Sels, B. F. *Energy Environ. Sci.* **2013**, *6*, 1415.

(17) Boronat, M.; Concepción, P.; Corma, A.; Renz, M.; Valencia, S. *J. Catal.* **2005**, *234*, 111–118.

(18) Bermejo-Deval, R.; Orazov, M.; Gounder, R.; Hwang, S. J.; Davis, M. E. *ACS Catal.* **2014**, *4*, 2288–2297.

(19) Harris, J. W.; Cordon, M. J.; Di Iorio, J. R.; Vega-Vila, J. C.; Ribeiro, F. H.; Gounder, R. *J. Catal.* **2016**, *335*, 141–154.

(20) Hayes, M. L.; Pennings, N. J.; Serianni, A. S.; Barker, R. *J. Am. Chem. Soc.* **1982**, *104*, 6764–6769.

(21) Assary, R. S.; Curtiss, L. A. *J. Phys. Chem. A* **2011**, *115*, 8754–8760.

(22) Bermejo-Deval, R.; Assary, R. S. S.; Nikolla, E.; Moliner, M.; Román-Leshkov, Y.; Hwang, S.-J. S.-J.; Palsdottir, A.; Silverman, D.; Lobo, R. F. F.; Curtiss, L. a. a.; Davis, M. E. E.; Roman-Leshkov, Y.; Hwang, S.-J. S.-J.; Palsdottir, A.; Silverman, D.; Lobo, R. F. F.; Curtiss, L. a. a.; Davis, M. E. E. *Proc. Natl. Acad. Sci. U.S.A.* **2012**, *109* (25), 9727–9732.

(23) Choudhary, V.; Caratzoulas, S.; Vlachos, D. G. *Carbohydr. Res.* **2013**, *368*, 89–95.

(24) Yang, G.; Pidko, E. a.; Hensen, E. J. M. *ChemSusChem* **2013**, *6*, 1688–1696.

(25) Rai, N.; Caratzoulas, S.; Vlachos, D. G. *ACS Catal.* **2013**, *3*, 2294–2298.

(26) Li, Y. P. P.; Head-Gordon, M.; Bell, A. T. T. *ACS Catal.* **2014**, *4*, 1537–1545.

(27) Christianson, J. R.; Caratzoulas, S.; Vlachos, D. G. *ACS Catal.* **2015**, *5*, 5256–5263.

(28) Shetty, S.; Pal, S.; Kanhere, D. G.; Goursot, A. *Chem. - A Eur. J.* **2005**, *12*, 518–523.

(29) Courtney, T. D.; Chang, C.-C.; Gorte, R. J.; Lobo, R. F.; Fan, W.; Nikolakis, V. *Microporous Mesoporous Mater.* **2015**, *210*, 69–76.

(30) Boronat, M.; Concepción, P.; Corma, A.; Navarro, M. T.; Renz, M.; Valencia, S. *Phys. Chem. Chem. Phys.* **2009**, *11*, 2876–2884.

(31) Bare, S. R.; Kelly, S. D.; Sinkler, W.; Low, J. J.; Valencia, S.; Corma, A.; Nemeth, L. T.; Modica, F. S.; Valencia, S.; Corma, A.; Nemeth, L. T. *J. Am. Chem. Soc.* **2005**, *127*, 12924–12932.

(32) Quadrelli, E. A.; Basset, J. M. *Coord. Chem. Rev.* **2010**, *254*, 707–728.

(33) Beletskiy, E. V; Hou, X.; Shen, Z.; Gallagher, J. R.; Miller, J. T.; Wu, Y.; Li, T.; Kung, M. C.; Kung, H. H. *J. Am. Chem. Soc.* **2016**, *138,* 4294–4297.

(34) Beletskiy, E. V; Shen, Z.; Riofski, M. V; Hou, X.; Gallagher, J. R.; Miller, J. T.; Wu, Y.; Kung, H. H.; Kung, M. C. *Chem. Commun.* **2014**, *50*, 15699–15701.

(35) Brand, S. K.; Labinger, J. A.; Davis, M. E. *ChemCatChem* **2016**, *8*, 121–124.

(36) Brand, S. K.; Josephson, T. R.; Labinger, J. A.; Caratzoulas, S.; Vlachos, D. G.; Davis, M. E. *J. Catal.* **2016**, *341*, 62–71.

(37) Zhao, Y.; Truhlar, D. G. *Theor. Chem. Acc.* **2008**, *120*, 215–241.

(38) Wadt, W. R.; Hay, P. J. *J. Chem. Phys.* **1985**, *82*, 284–298.

(39) Frisch, M. J.; Trucks, G. W.; Schlegel, H. B.; Scuseria, G. E.; Robb, M. A.; Cheeseman, J. R.; Scalmani, G.; Barone, V.; Mennucci, B.; Petersson, G. A.; Nakatsuji, H.; Caricato, M.; Li, X.; Hratchian, H. P.; Izmaylov, A. F.; Bloino, J.; Zheng, G.; Sonnenberg, J. L.; Hada, M.; Ehara, M.; Toyota, K.; Fukuda, R.; Hasegawa, J.; Ishida, M.; Nakajima, T.; Honda, Y.; Kitao, O.; Nakai, H.; Vreven, T.; Montgomery Jr., J. A.; Peralta, J. E.; Ogliaro, F.; Bearpark, M. J.; Heyd, J.; Brothers, E. N.; Kudin, K. N.; Staroverov, V. N.; Kobayashi, R.; Normand, J.; Raghavachari, K.; Rendell, A. P.; Burant, J. C.; Iyengar, S. S.; Tomasi, J.; Cossi, M.; Rega, N.; Millam, N. J.; Klene, M.; Knox, J. E.; Cross, J. B.; Bakken, V.; Adamo, C.; Jaramillo, J.; Gomperts, R.; Stratmann, R. E.; Yazyev, O.; Austin, A. J.; Cammi, R.; Pomelli, C.; Ochterski, J. W.; Martin, R. L.; Morokuma, K.; Zakrzewski, V. G.; Voth, G. A.; Salvador, P.; Dannenberg, J. J.; Dapprich, S.; Daniels, A. D.; Farkas, Ö.; Foresman, J. B.; Ortiz, J. V; Cioslowski, J.; Fox, D. J. Gaussian 09, 2009.

(40) Glendening, E. D.; Landis, C. R.; Weinhold, F. *J. Comput. Chem.* **2013**, *34*, 1429–1437.

(41) Bader, R. F. W. *Atoms in Molecules - A Quantum Theory;* Oxford University Press: Oxford, England, 1990.

(42) Otero-De-La-Roza, A.; Johnson, E. R.; Luaña, V. *Comput. Phys. Commun.* **2014**, *185*, 1007–1018.

(43) Taylor, M. J.; Coddington, J. M. *Polyhedron* **1992**, *11*, 1531–1544.

(44) Kozuch, S. *ACS Catal.* **2015**, *5*, 5242–5255.

(45) Curtin, D. Y. *Rec. Chem. Prog.* **1954**, *15*, 111–128.

Table of Contents Image / Graphical Abstract